Available online at www.sciencedirect.com
ScienceDirect
Journal of Non-Crystalline Solids 354 (2008) 2495–2499
JOURNAL OF NON-CRYSTALLINE SOLIDS
www.elsevier.com/locate/jnoncrysol

Theoretical study of an amorphous chalcogenide surface

F. Inam, D.A. Drabold *

Department of Physics and Astronomy, Ohio University, Athens, OH 45701, USA

Available online 20 February 2008

Abstract

The structure of amorphous surfaces is a challenging frontier yet to be thoroughly explored. Standard surface characterization techniques like STM are difficult to apply to these surfaces. We have studied $GeSe_2$ glass surfaces using first principle methods in a slab geometry. The glass surfaces are obtained by quenching a slab of an equilibrated liquid. We have found that these surfaces are well characterized by the distribution of rings. A detailed study of ring formation and associated properties is presented. We also briefly describe the electronic/optical and vibrational structure of these surfaces.

PACS: 61.43.Fs; 68.03.Hj

Keywords: Chalcogenides; Density functional theory; Structure; Surfaces and interfaces

1. Introduction

The binary chalcogenide glass g-$GeSe_2$ has been extensively studied for its structural and optical properties. The microscopic nature of atomic order beyond the nearest neighbor distances has long been a controversial subject. There are two main approaches which address the structure. One is the chemically ordered covalent random network approach, first developed by Zachariasen [1] and later used by Tronc et al. [2] to interpret their optical-absorption edge and Raman-scattering results on Ge_xSe_{1-x} alloys. In this model chemically wrong bonds are forbidden. Another approach is by Bridenbaugh et al. [3]. It explains ordering as arising from a quasi-ordered structural unit, presumably a reminiscent of a crystalline phase, in which wrong bonds exist as an integral part. The presence of chemical disorder has been experimentally confirmed by Boolchand et al. [4] and Petri et al. [5]. The first principle molecular dynamics model of g-$GeSe_2$ by Cobb et al. [6] also reports a significant fraction of homopolar bonds. Concentration of wrong bonds in these models is found to vary when such models are relaxed under different pressures [7]. Ge–Ge bonds are found to be relatively unstable under pressure as compared to Se–Se bonds.

Surface properties of g-$GeSe_2$ are relatively less known. Experimental surface techniques like STM have been applied to a-C:H [8] thin films and a-Si:H surfaces [9] with some success, but it is difficult to apply these techniques to amorphous surfaces in general. Simulations of amorphous solid surfaces can be divided into two categories, molecular dynamics (MD) simulations based on semiempirical potentials and first principle methods. Earlier work by Garofalini [10,11] on amorphous silica surfaces, using classical MD techniques provides a basic understanding of amorphous surfaces. Similar methods were used to study other amorphous oxides like Al_2O_3 [12]. In the last decade some calculations were reported on first principle modeling of surfaces of a-Si [13], a-Si:H [13], liquid-Si, [14], a-C [15,16] and g-$GeSe_2$ [17]. In most of these studies, the scheme used to form a surface is same as is used for crystalline surface; minimizing the total energy of the supercell with boundary conditions applied in two directions only, leaving two free unreconstructed surfaces. This scheme, though successful in the study of crystalline surfaces, has

* Corresponding author.
E-mail addresses: drabold@ohio.edu, drabold@helios.phy.ohiou.edu (D.A. Drabold).

0022-3093/$ - see front matter © 2008 Elsevier B.V. All rights reserved.
doi:10.1016/j.jnoncrysol.2007.09.118

a disadvantage. It is able to explore only a limited class of configurations near the truncated bulk.

In this paper, we present first principle MD simulation of the surface of glassy $GeSe_2$ using quench from melt technique, which is found successful in modeling bulk glasses [6,18]. Starting with an equilibrated liquid with two free surfaces, the glass slab is obtained, which shows the outer layers reconstructed by the formation of rings of different sizes bundled together. Coordination statistics show improved bond configurations. Vibrational spectra of the slab reveals the mixing of A_1 and optical band due to a slight increase in the Ge–Se bond length.

2. Constraints on theory

Simulations were carried out using the density functional local basis *ab initio* code 'Fireball' [19]. The starting point of our work is a 216 atom cubic (18.76 Å) bulk model by Cobb et al. [6] showing reasonable agreement with the experiment. To construct a surface model we joined two copies of the Cobb cell in the z-direction to get a parallelepiped cell of 432 (144 Ge and 288 Se) atoms. In this way we get reasonable thickness in the z-direction. The system is relaxed in the slab geometry by breaking the periodicity in the z-direction to get a 'relaxed' truncated bulk. It is then melted in the slab geometry at $T \simeq 1100$ K. The liquid phase is obtained by equilibrating the system at this temperature for 8 ps using microcanonical molecular dynamics with a time step of 2.5 fs. To obtain the amorphous phase, the liquid slab was slowly cooled to room temperature (270 K) over a period of 7.5 ps. After equilibration for 2.5 ps, it was quenched to 0 K.

The total energy of the resulting slab is 37 meV/atom lower than that of the relaxed truncated bulk. Annealing at high temperature caused the system to expand from the initial bulk thickness in the z-direction. Fig. 1 plots the local density in the slab and bulk along z-axis. Upper and bottom layers are shown in Fig. 2.

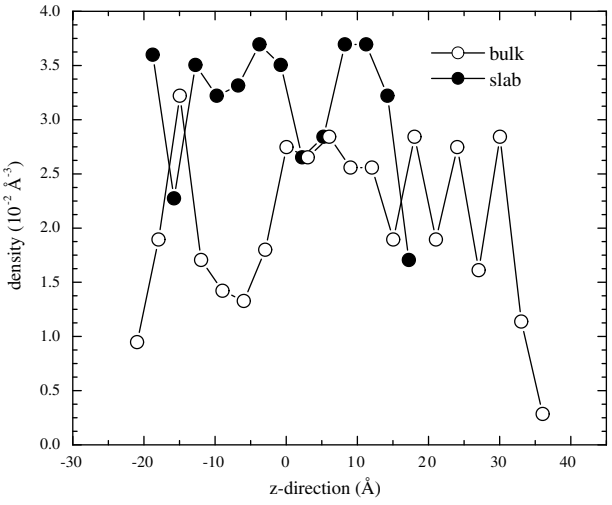

Fig. 1. Density fluctuations in bulk and slab. Atoms are counted in layers of 3.0 Å width along the z-axis.

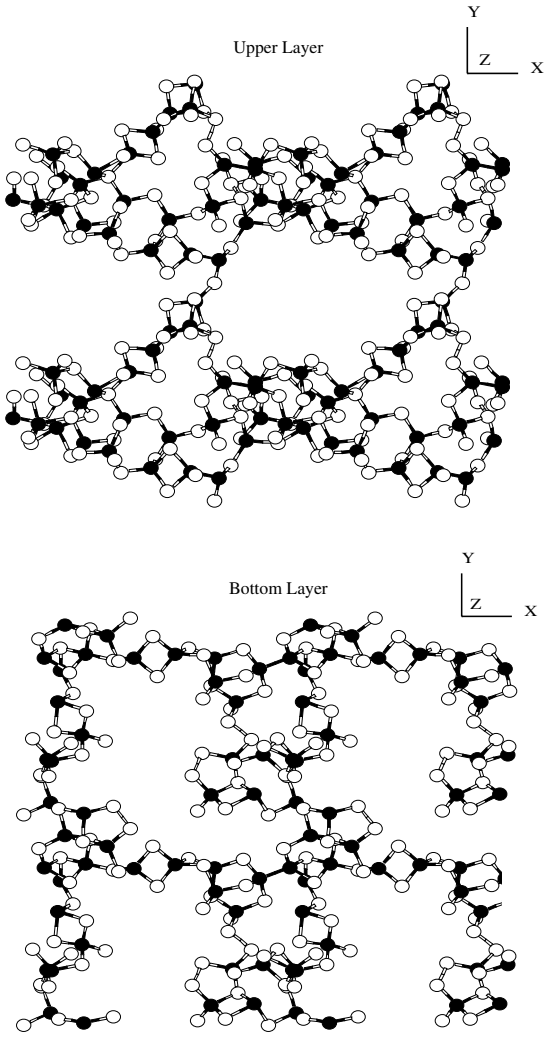

Fig. 2. Upper and bottom surfaces (8 Å thick) of the slab are shown. Filled circles represent Ge atoms and empty circles represent Se. Periodic boundary conditions are used to reveal four copies of the layers in the xy plane to emphasize the ring network.

3. Coordination and ring statistics

Overall, coordinate statistics do not differ significantly between the surface and bulk. Both chemical ordering and the 8-N rule is some what better satisfied on the upper and bottom layers relative to the interior of the slabs. Homopolar Ge–Ge bonds are decreased to 1.4% of the total number of possible bonds ($4N/3$, N is the number of atoms in the system) when bonding criteria for Ge and Se is satisfied, as compared to 3.5% Ge–Ge bonds present in the bulk. Similarly Se–Se bonds are decreased to 6% from 8% bonds in the bulk model. This seems consistent with the pressure induced effect on this system as studied by Durandurdu et al. [7]. The reason could be that quenching the system in the slab geometry is thermodynamically similar to the quenching under constant pressure. Such

Table 1
A comparison between n-fold rings in bulk and slab model

n	3	4	5	6	7	8	9	10
Bulk	6	40	20	44	4	18	14	8
Slab	0	44	23	47	12	29	12	20

improvement in the chemical order has directly affected the ring structure of the system.

Table 1 compares the number of different size rings in the slab to that in the bulk. The number of rings has increased relative to bulk, with specific increase in the even size rings as compared to odd size rings, which is the consequence of the decrease in the homopolar bonds. Upper and bottom layers are characterized by the formation of rings of different sizes attached together as shown in Fig. 2. About 94% of the atoms in these layers constitute the ring network.

4. Structural properties

Structural properties of the glass slab are studied by calculating the pair correlation functions $g(r)$ and static structure factors $S(K)$. To study the contributions to $S(K)$ from different parts of the slab, we split the slab into different regions and calculate $g(r)$ and $S(K)$ locally. To study the signature of rings in the structural properties of the slab, we selected atoms which are part of rings of sizes 4–10, and calculated the static structure factor including only these atoms. Fig. 3 shows the comparison of $S(K)$ for both sets of atoms. Atoms which are not part of these rings contribute relatively more at $K = 2.0$ Å^{-1} to the total structure factor of the slab as compared to ring atoms, while the rest of the spectrum is dominated by the contribution from the atoms which are part of rings. Fig. 4 shows total $g(r)$ of the new slab, 'relaxed' slab and of the bulk model. The first peak for both the new and 'relaxed' slab is increased to 2.44 Å and 2.43 Å, respectively as compared to 2.35 Å for the bulk model. For the new slab, heights of first and second peaks are increased considerably as compared to that of relaxed truncated bulk and bulk model, which is a direct consequence of increase in the Ge–Se bonds and increase in the number of rings. Fig. 5 shows the contribution to the total $g(r)$ of the slab from the upper, bottom and inner regions. Increase in the height of first peak for upper and bottom layer shows an increase of Ge–Se bonds on outer layers as compared to the inner region. At larger distances these layers show some small peaks which are suppressed in the inner region. These peaks correspond to rings attached to each other. Structural analysis of the slab reveals an enhancement of atomic ordering at larger distances on outer layers due to the appearance of ring network.

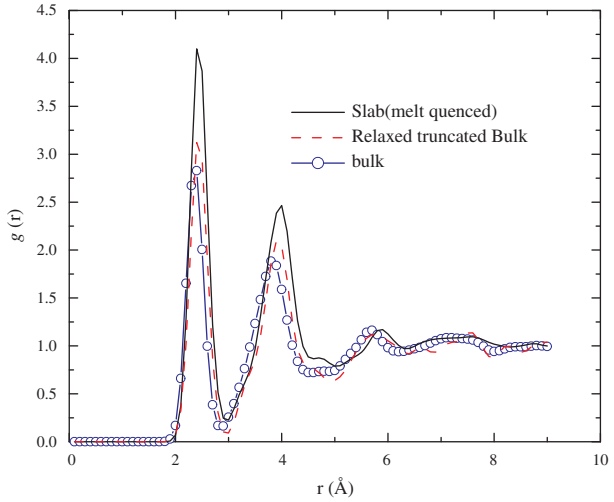

Fig. 4. Total $g(r)$ of new slab model is compared with that of 'relaxed' truncated glass slab and bulk model.

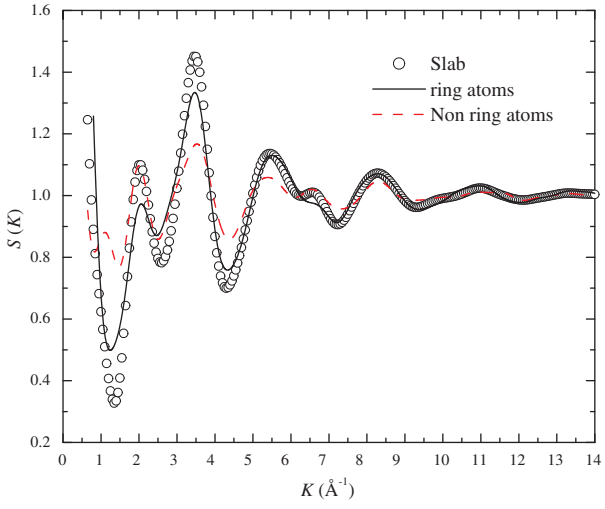

Fig. 3. $S(K)$ calculated from the atoms which are part of rings of sizes 4–10, and from the atoms which are not part of these rings. The two curves are compared to $S(K)$ from the whole slab.

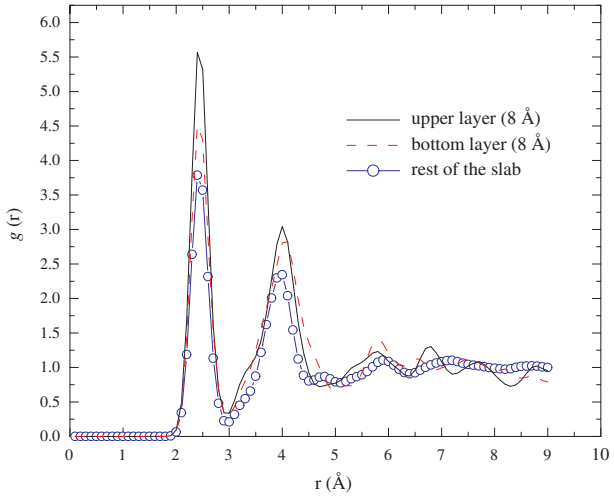

Fig. 5. $g(r)$ of the upper bottom and interior region of the new slab model.

5. Vibrational density of states and normal modes

Dynamical properties of the slab model are studied by calculating the vibrational density of states (VDOS). The normal mode spectrum is determined from the dynamical matrix, which is obtained by displacing each atom by *0.03* Å in three orthogonal directions and performing first principle force calculation to obtain the force constant matrix. A comparison is made with the vibrational properties of the bulk $GeSe_2$ 63 atom model [20], which shows reasonable agreement with the experiment on the bulk. Fig. 6 shows the vibrational density of states (VDOS) for both bulk and the slab. As compared to the VDOS of the bulk model, the middle A_1 band and the optical band is mixed for the slab, while the acoustic band follows nearly the same profile as that of bulk. The reason for this change at higher modes lies in the increase of Ge–Se bond lengths as compared to that of bulk. Higher modes are characterized by stronger localization as compared to extended lower modes. Due to the increase in the Ge–Se bond lengths, the localization of higher modes is decreased and the over all distribution weight is shifted towards the lower modes. The effect is similar to what was reported by Cobb and Drabold [21] for liquid bulk $GeSe_2$, which shows a similar mixing of the two bands.

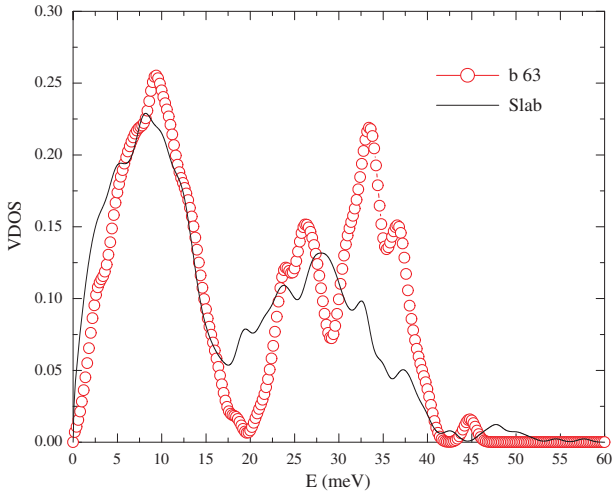

Fig. 6. Vibrational density of states of the slab and bulk [20] (63 atom) models.

6. Electronic properties

The electronic density of states (Fig. 7(a)) looks similar to that of bulk. In order to analyze the physical nature of eigenstates, we calculated the Mulliken charge at each atomic site for each eigenstate. For each eigenstate n, we define an average charge Q_n^{α} accumulated on atomic site 'α'. Fig. 7(b) and (c) shows the charge spectrum for Ge and Se, respectively. It is interesting to note that the average charge on Ge sites is increased at valence and conduction tails, compared to Se sites. It suggests that the localization at the band tails is due mainly to Ge sites. Charge on Ge sites is found to be effected by the geometrical defects. Threefold Ge show larger average bond length 2.46 Å, as compared to 2.44 Å for 4-fold Ge, with larger angle deviations from the tetrahedra angle 109.4° ranging from 78° to 94°. Threefold Ge sites are found to be the main contributors to the total charge for valence tail eigenstates. Fourfold Ge sites with average bond lengths ranging from 2.44 Å to 2.45 Å mainly contribute to the total charge corresponding to conduction tails.

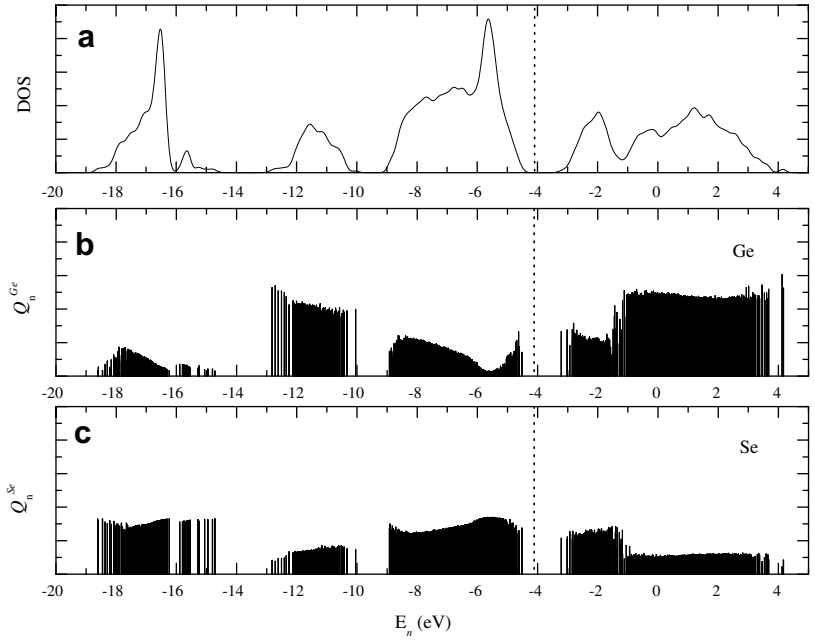

Fig. 7. (a) Electronic density of states for the whole slab. Dotted line shows the position of fermi level. (b) and (c) shows the Mulliken charge on Ge and Se sites, respectively.

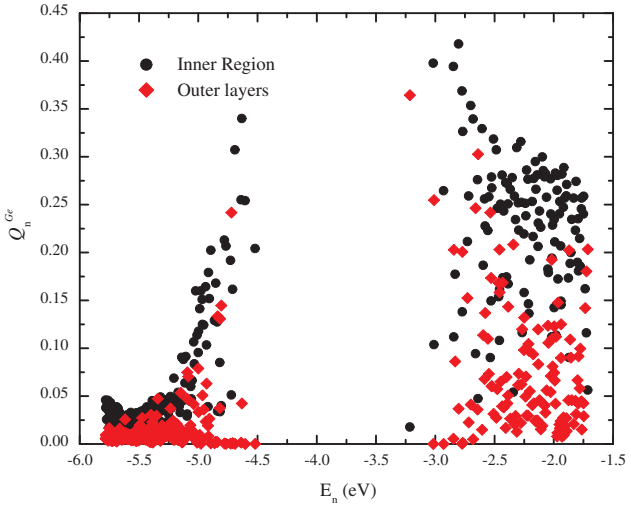

Fig. 8. Q_n accumulated on Ge sites in outer and inner regions of the slab for valence and conduction band edges.

Ge atoms on the upper and bottom layers (8 Å thickness) show more ideal coordination statistics. Only 24% of the total threefold Ge present in the upper and bottom layers of the slab. As we have mentioned before, the localization at the valence tail is mostly contributed by threefold Ge, thus the surface atoms show (Fig. 8) less average charge accumulation for the valence tail as compared to the atoms in the interior. This decrease in the coordination defects stands in contrast to the general understanding of crystalline surfaces, where defect density increases at the surface due to the increase in the concentration of the dangling bonds, which results in the increase in localized states. In crystalline case, surface atomic positions are less affected by the neighboring network as compared to the amorphous phase where the local network is more random and adopts more to allow the surface to minimize its energy. On the crystalline surface, atoms being less diffusive tend to settle in a local minimum energy configuration in under coordinated state. This is different in case of glassy slab obtained through annealing and quenching which allows the species to diffuse more, and thus they are able to scan the larger energy configuration space, hence settle in a better coordination state.

7. Conclusion

We have modeled the g-$GeSe_2$ surface using quench from melt method in the slab geometry. Structural properties of the new slab model is compared with the slab generated by the conventional relaxation technique. The new model gives lower total energy per atom as compared to the relaxed model. It shows the decrease in homopolar bonds as compared to relaxed and bulk model. The outer layers of the slab are characterized by the rings of different sizes attached to each other, with relatively lower coordination and geometrical defects as compared to the inner region. Electronic density of states for the slab follows the same profile as that of bulk. Surface states did not appear in the gap. Due to the increase in the Ge–Se bond length, the vibration density of the slab shows a significant change for higher modes as compared to that of bulk.

Acknowledgements

DAD and FI thank the National Science Foundation for support under Grant Nos. DMR 0605890 and 0600073, and the NSF International Materials Institute for New Functionalities in Glass, DMR 0409588.

References

[1] W.H. Zachariasen, J. Am. Chem. Soc. 54 (1932) 3841.
[2] P. Tronc, M. Bensoussan, A. Brenac, C. Sebenne, Phys. Rev. B 8 (1973) 5947.
[3] P.M. Bridenbaugh, G.P. Espinosa, J.E. Griffiths, J.C. Phillips, J.P. Remeika, Phys. Rev. B 20 (1979) 4140.
[4] P. Boolchand, J. Grothaus, W.J. Breser, P. Suanyi, Phys. Rev. B 25 (1982) 2975.
[5] Ingrid Petri, Philip S. Salmon, Phys. Rev. Lett. 84 (2000) 2413.
[6] M. Cobb, D.A. Drabold, R.L. Cappelletti, Phys. Rev. B 54 (1996) 12162.
[7] Murat Durandurdu, D.A. Drabold, Phys. Rev. B 65 (2002) 104208-1.
[8] I. Rusman, L. Klibanov, L. Burstein, Yu. Rosenberg, V. Weinstein, E. Ben-Jacob, N. Croitoru, A. Seidman, Thin Solid Films 287 (1996) 36.
[9] J. Herion, K. Szot, Ch. Ross, F. Siebke, J. Non. Cryst. Sol 227–230 (1998) 78.
[10] S.M. Levine, S.H. Garofalini, J. Chem. Phys. 86 (1987) 2997.
[11] G.P. Feuston, S.H. Garofalini, J. Chem. Phys. 91 (1989) 564.
[12] S.P. Adiga, P. Zapol, L.A. Curtiss, Phys. Rev. B 74 (2006) 064204.
[13] K. Kilian, D.A. Drabold, J.B. Adams, Phys. Rev. B 48 (1993) 17393.
[14] G. Fabricius, E. Artacho, D. Sánchez-Portal, P. Ordejón, D.A. Drabold, J.M. Soler, Phys. Rev. B 60 (1999) R16283.
[15] J. Dong, D.A. Drabold, Phys. Rev. B 57 (1998) 15591.
[16] R. Haerle, G. Galli, A. Baldereschi, Appl. Phys. Lett. 75 (1999) 1718.
[17] X. Zhang, D.A. Drabold, Phys. Rev. B 62 (2000) 5695.
[18] D. Tafen, D.A. Drabold, Phys. Rev. B 71 (2005) 054206.
[19] A.A. Demkov, J. Ortega, O.F. Sankey, M. Grumbach, Phys. Rev. B 52 (1995) 1618;
O.F. Sankey, D.A. Drabold, A. Gibson, Phys. Rev. B 50 (1994) 1376.
[20] R.L. Cappelletti, M. Cobb, D.A. Drabold, W.A. Kamitakahara, Phys. Rev. B 52 (1995) 9133.
[21] M. Cobb, D.A. Drabold, Phys. Rev. B 56 (1997) 3054.